Drug Design, Development and Therapy

Dovepress
open access to scientific and medical research

Open Access Full Text Article

ORIGINAL RESEARCH

Co-Expression Network Analysis and Molecular Docking Demonstrate That Diosgenin Inhibits Gastric Cancer Progression via SLC1A5/mTORC1 Pathway

Ning Cui[1], Feng Ding[2]

[1]Department of Gastroenterology, Renmin Hospital of Wuhan University, Wuhan, People's Republic of China; [2]Department of Gastroenterology, Zhongnan Hospital of Wuhan University, Wuhan, People's Republic of China

Correspondence: Feng Ding, Email dingfengkt@163.com

Background: Tumor-Node-Metastasis (TNM) stage of gastric cancer (GC) is one of the main factors affecting clinical outcome. The aim of this study was to explore the targets related to TNM stage of GC, and screening natural bioactive drug.

Methods: RNA sequencing data of the TCGA-STAD cohort were downloaded from UCSC database. Genes associated with TNM staging were identified by weighted gene co-expression network analysis (WGCNA). Univariate Cox regression, least absolute shrinkage and selection operator (LASSO), extreme gradient boosting (Xgboost), random forest (RF) and cytohubba plug-in of cytoscope were applied to screen hub genes. Natural bioactive ingredients were available from the HERB database. Molecular docking was used to evaluate the binding activity of active ingredients to the hub protein. CCK-8, flow cytometry, transwell and Western blot assays were used to analyze the effects of diosgenin on GC cells.

Results: 898 TNM-related genes were screened out through WGCNA. Three genes associated with GC progression/prognosis were identified, including nuclear receptor subfamily 3 group C member 2 (NR3C2), solute carrier family 1 member 5 (SLC1A5) and FAT atypical cadherin 1 (FAT1) based on the machine learning algorithms and hub co-expression network analysis. Diosgenin had good binding activity with SLC1A5. SLC1A5 was highly expressed in GC and was closely associated with tumor stage, overall survival and immune infiltration of GC patients. Diosgenin could inhibit cell viability and invasive ability, promote apoptosis and induce cell cycle arrest in G0/G1 phase. In addition, diosgenin promoted cleaved caspase 3 expression and inhibited Ki67, cyclin D1, p-S6K1, and SLC1A5 expression levels, while the mTORC1 activator (MHY1485) reversed this phenomenon.

Conclusion: For the first time, this work reports diosgenin may inhibit the activation of mTORC1 signaling through targeting SLC1A5, thereby inhibiting the malignant behaviors of GC cells.

Keywords: gastric cancer, weighted gene co-expression network analysis, diosgenin, molecular docking, diosgenin

Introduction

Gastric cancer (GC) is one of the leading causes of cancer-related death worldwide.[1] As a highly aggressive tumor with heterogeneity, GC still poses a global health problem.[2] There are an estimated 19.3 million new cancers worldwide, and GC accounts for 7.7% of cancer deaths.[3] The 5-year survival rate of GC patients with advanced GC is not obviously improved in last decades.[4] Tumor Node Metastasis (TNM) staging system is the cornerstone of prognostic prediction and treatment decision in GC, which indicates the status of disease progression.[5–7] There is an urgent need to explore the biological mechanisms that influence the TNM staging of GC, which may help to develop new therapeutic agents.

Diosgenin is a kind of natural steroid saponin, which is widely found in a variety of plants, such as *Trigonella foenum-graecum, Dioscorea and Polygonati Rhizoma*.[8–10] Diosgenin shows potential to treat human diseases, such as diabetes, hypercholesterolemia, and gastrointestinal disorders.[11–13] Importantly, some recent studies have shown that diosgenin plays a tumor-suppressive role in various cancers, including GC,[14,15] and its functions through anti-inflammation, anti-proliferation,

Received: 9 April 2024
Accepted: 10 July 2024
Published: 23 July 2024

pro-apoptosis, and inhibition of epithelial-mesenchymal transition.[16–18] However, the function and mechanism of diosgenin in GC has not been fully elucidated.

Weighted gene co-expression network analysis (WGCNA) is a systematic bioinformatics algorithm capable of combining co-expressed genes into several gene modules and providing insights into signal transduction networks that may be responsible for tumor progression.[19] At present, WGCNA has been used to explore the correlation between clinical features of diseases and gene clusters.[20,21] It is widely used to identify candidate biomarkers or therapeutic targets for multiple cancers.[22–25]

In this study, WGCNA, random forest (RF), least absolute shrinkage and selection operator (LASSO) and extreme gradient boosting (XGBoost) were applied to obtain the crucial genes including nuclear receptor subfamily 3 group C member 2 (NR3C2), solute carrier family 1 member 5 (SLC1A5) and FAT atypical cadherin 1 (FAT1), which were associated with TNM stage of GC patients. Additionally, molecular docking and in vitro assays were applied to validate that, diosgenin targeted SLC1A5, to inhibit the malignant biological behaviors of GC cells.

Methods and Materials

In silico Data Collection

Through UCSC database (https://xenabrowser.net/datapages/), TCGA stomach adenocarcinoma (STAD) dataset of RNAseq data (dataset ID: TCGA-STAD.htseq_fpkm.tsv, including 407 samples), ID/Gene Mapping (gencode. V22. An annotation. Gene. ProbeMap) and phenotype files (dataset ID: TCGA - STAD. GDC_phenotype. TSV. includes 544 samples) were downloaded.

Wgcna

R package "WGCNA" was applied to create a gene co-expression network for GC according to the methodology reported by a previous study.[19] In brief, firstly, the samples are clustered to evaluate if there were any obvious outliers. Then, the co-expression network was constructed. The soft threshold power β was calculated using the pickSoftThreshold, and the co-expression similarity was improved to calculate the adjacency. Then, hierarchical clustering and dynamicTreeCut were used to detect the module. Finally, gene significance (GS) and module membership (MM) were calculated to correlate modules with clinical feature to identify clinically relevant modules.

Functional Enrichment Analysis

The genes in the target module were extracted. With DAVID database (https://david.ncifcrf.gov/summary.jsp), gene ontology (GO) analysis and Kyoto Encyclopedia of Genes and Genomes (KEGG) analysis were performed to identify the functional properties of the gene set.[26] Finally, visualization was performed on Sangerbox platform.[27]

Core Gene Screening

Univariate Cox analysis was performed by combining the target module genes with survival information through survival R package. Graphing was performed with Sangerbox platform.[27] According to the results of Univariate Cox analysis, R packages including randomForestSRC,[28] glmnet[29] and xgboost[30] were applied to perform analyses based random forest (RF), least absolute shrinkage and selection operator (LASSO) and extreme gradient boosting (XGBoost), respectively. The genes in the intersection were obtained by R-package "ggvenn", which were regarded as the core genes.

Protein-Protein Interaction Network Construction

GeneMANIA (http://www.genemania.org) is a website for building protein-protein interaction (PPI) networks that can be used to generate gene function predictions.[31] In the present work, PPI network was visualized by cytoscope 3.9.1 software, and topological analysis was carried out by calculating the betweenness (BC), degree (DC), closeness (CC), Maximal Clique Centrality (MCC) of these genes with cytoHubba plug-in.[32]

Acquisition and Screening of Natural Ingredients

HERB database (http://herb.ac.cn/) was applied to find natural ingredients associated with specific targets and GC. TCMSP (https://tcmsp-e.com/index.php) and SwissADME (http://www.swissadme.ch/) databases were used to search for the pharmacological and molecular properties of these ingredients, and oral bioavailability (OB) greater than 30%, drug-likeness (DL) greater than 0.18, high gastrointestinal (GI) absorption, and "Yes, 0 violation" in DL analysis were applied to screen active ingredients.

Molecular Docking

Mol2 format files of bioactive ingredients were obtained from TCMSP database. The PDB files of SLC1A5 (PDB ID: 5LM4) and NR3C2 (PDB ID: 3WFG) were obtained from the PDB database (https://www.rcsb.org/). The proteins and molecules were dehydrated and hydrotreated with AutoDockTools-1.5.7 software and set as receptors and ligands, respectively. Then, AutoDock Vina was used to obtain the docking result, and the best binding mode was selected according to the minimum binding energy. Finally, Pymol software was used to visualize the docking results and outport 3D images.

Gene Set Enrichment Analysis (GSEA)

h.all.v7.4.symbols.gmt dataset was downloaded from Molecular Signatures Database (MSigDB, https://www.gsea-msigdb.org/gsea/index.jsp). According to the median expression of SLC1A5 in the samples of TCGA-STAD dataset, the samples were divided into high expression group and low expression group. The minimum gene set size was set to 5 and the maximum gene size was set to 5000, and nperm was set to 1000. The normalized enrichment score (NES) is the main statistic for examining the enrichment results of gene sets. The false discovery rate (FDR) is the estimated probability that a set of genes with a given NES represents a false-positive finding. We selected NES and FDR as enrichment indicators (gene sets with $|NES|>1$ and $FDR< 0.25$ were considered to be significantly enriched).

Immunohistochemistry

The tumor tissues and para-cancer tissues of GC patient were embedded in paraffin and cut into 5 μm sections. The sections were stained by indirect immunoperoxidase method. Briefly, the sections were incubated with recombinant anti-SLC1A5 antibody (1:100; ab251591; Abcam, Shanghai, China) overnight in a wet box at 4°C. The next day, the sections were incubated with a secondary goat anti-rabbit IgG H&L antibody (1:1000, ab150077, Abcam, Shanghai, China) at room temperature in a wet box for 30 min. The sections were then stained with diaminobenzidine and observed under a microscope.

Cell Culture

Human GC cell lines AGS (CRL-1739) and SNU-16 (CRL-5974) were obtained from American Type Culture Collection (ATCC, Rockville, MD, USA). AGS is a cell line exhibiting epithelial morphology that was isolated in 1979 from the stomach tissue of a 54-year-old, White, female patient with gastric adenocarcinoma. SNU-16 is a cell line exhibiting epithelial morphology that was isolated in 1987 from ascites derived from a 33-year-old, female, Asian, GC patient prior to chemotherapy. The GC cells were cultured in a humidified atmosphere at 37 °C containing 95% air and 5% CO_2, and cultured in RPMI-1640 medium (Sigma-Aldrich, St. Louis, MO, USA) containing 10% heat-inactivated fetal bovine serum (FBS) (Sigma-Aldrich, St. Louis, MO, USA), 100U/mL penicillin and 0.1 mg/mL streptomycin. Experiments were performed using the cells in the logarithmic growth stage.

Diosgenin (HY-N0177, MCE China, Shanghai, China) and MHY1485 (HY-B0795, MCE China, Shanghai, China) were dissolved in methyl sulfoxide (DMSO), diluted with complete medium, and were applied to treat GC cells. The cells were divided into four groups: 10 μM diosgenin treatment group, 20 μM diosgenin treatment group, 20 μM diosgenin + 10 μM MHY1485 group, and the control group.

Cell Viability Assay

Cell viability was assessed using cell counting kit −8 (CCK-8, Dojindo, Kumamoto, Japan). The cells were inoculated in 96-well plates (3×10^5 cells/well) and treated with diosgenin and MHY1485 at 37°C for 48 h. The cells were then

incubated with 10 μL CCK-8 at 37 ° C for another 2 h. The absorbance was measured by a microplate reader at a wavelength of 450nm.

Flow Cytometry

Apoptosis of GC cells was measured using an Annexin V-FITC/PI apoptosis kit (BD Biosciences, San Jose, CA, USA) according to the manufacturer's instruction. In short, GC cells were washed with phosphate buffer saline (PBS) and re-suspended in 100 μL binding buffer. Annexin V-FITC (5 μL) was then added and the cell suspension was incubated in the dark for 5 min, and then the GC cells were incubated in the dark with 5 μL propidium iodide. After the cells were washed with binding buffer, the fluorescence intensity was measured by a flow cytometer (FACSCalibur, BD Biosciences, San Jose, CA, USA).

To detect cell cycle progression, GC cells were washed twice with PBS, fixed with 70% ethanol, and stored overnight at 4°C. The cells were then treated with 1mg/mL RNase A at 37°C for 30 min and then stained with 50μg/mL propidium iodide in the dark for 15 min. After the cells were washed with PBS, cell cycle was evaluated by the flow cytometer.

Transwell Assay

The invasion of cells was assessed by matrigel-coated transwell chambers (8 μm pore size; Corning, Beijing, China). The cells were resuspended in serum-free RPMI-1640 medium, and the cell density was adjusted to 5×10^4 cells /mL. Then, 100 μL cell suspension was added into the upper chamber. 600 μL medium containing 10% FBS was added to the lower chamber. Then the cells were treated with diosgenin and MHY1485. After 24 h of culture, the invading cells were fixed and stained with crystal violet solution. After the membrane was washed, the number of invading cells were counted and photographed in five fields under an inverted microscope.

Western Blot

For each sample, GC cells were lysed in 200 μL of RIPA lysis buffer. The protein concentration was determined by Bradford method. The same amount of protein in each group was separated by sodium dodecyl sulfate-polyacrylamide gel electrophoresis (SDS-PAGE), and then transferred to polyvinylidene fluoride membranes (PVDF) (Millipore, Bedford, MA, USA). Subsequently, the PVDF membranes was blocked for 1h with 5% skim milk at room temperature. The PVDF membranes were then incubated with anti-Ki67 antibody (1:1000, ab16667, Abcam, Shanghai, China) and anti-cleaved caspase-3 antibody (1:1000, ab2302, Abcam, Shanghai, China). Anti-Cyclin D1 antibody (1:1000, ab134175, Abcam, Shanghai, China), anti-phospho-T229 S6K1 antibody (1:1000, ab59208, Abcam, Shanghai, China), anti-SLC1A5 antibody (1:1000, ab187692, Abcam, Shanghai, China) and anti-glyceraldehyde 3-phosphate dehydrogenase (GAPDH) antibody (1:1000, ab9485, Abcam, Shanghai, China) at 4 °C overnight. The next day, the membrane was washed and incubated with horseradish peroxide-coupled secondary antibodies (1: 5000, Abcam, Shanghai, China) at room temperature for 2 h. The protein markers (LC5625, 26,619, 26634, LC5699) were purchased from ThermoFisher Science (Rockford, IL, USA). The signal was visualized using a chemiluminescence detection system (ChemiDoc Touch, BioRad).

Statistical Analysis

All statistical analyses were performed using GraphPad Prism 7.0 software. The data are expressed as "mean ± standard deviation (SD)". Differences between two or among more groups were analyzed using *T*-test or one-way analysis of variance (ANOVA). P values < 0.05 were considered to be statistically significant.

Results

Co-Expression Network Construction and Module Identification

The gene expression matrix was obtained by processing the TCGA-STAD data. The top 5000 genes with differential expression were then selected for further analysis. In addition, clinical data (543 samples) were extracted after excluding patients with incomplete clinical information. Soft threshold was set to 5 to construct a scale-free network (Figure 1A). Nine modules were obtained by combining strongly related modules (Figure 1B-C). And there were no significant

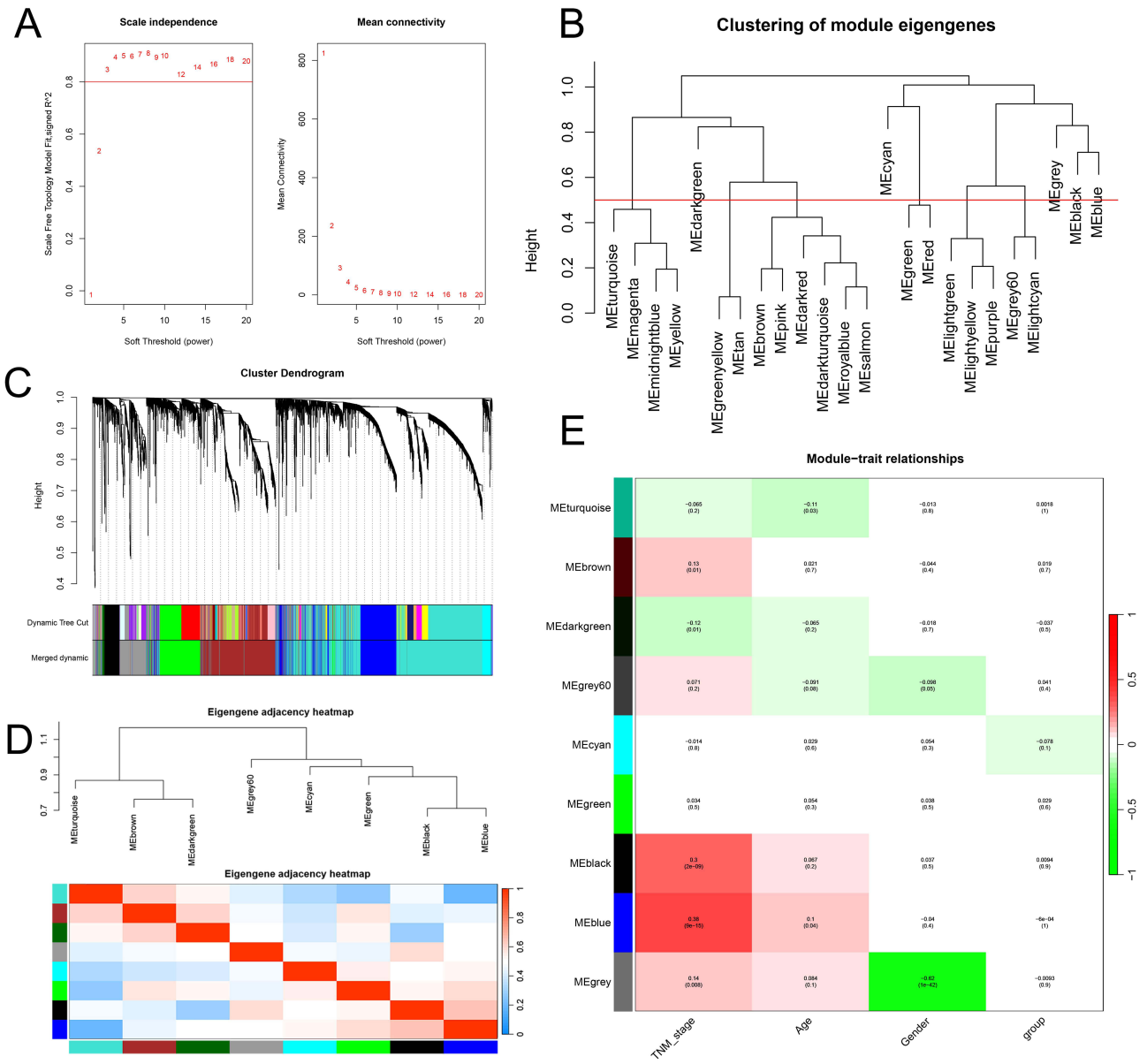

Figure 1 WGCNA with TCGA-STAD cohort. (**A**) Scale Independence and mean connectivity in TCGA-STAD cohort. (**B**)Clustered dendrograms were cut at a height of 0.5 to detect and combine similar modules. (**C**) Cluster trees and modules of co-expressed genes. (**D**) Eigengene dendrogram and eigengene adjacency plot. Red indicates a high correlation and blue indicates the opposite result. (**E**) Pearson correlation analysis between modules and TNM stage, age, gender and group.

correlations among the modules (Figure 1D). The blue and black modules were highly correlated with TNM staging (Figure 1E), so the genes in these two modules were considered to be clinically meaningful.

GO and KEGG Analyses of the Genes in Blue and Black Modules

The genes of blue and black modules were extracted. The results of GO analysis showed that genes were mainly enriched in cell division (GO:0051301), cell cycle (GO:0007049), and DNA replication (GO:0006260). For cell components, the genes were mainly enriched in nucleoplasm (GO:0005654), nucleus (GO:0005634), and chromosome (GO:0005694). For molecular function, genes were mainly enriched in ATP binding (GO:0005524), protein binding (GO:0005515), and ATPase activity (GO:0016887) (Figure 2A). KEGG analysis showed that these genes were mainly about Cell cycle (hsa04110), DNA replication (hsa03030), and p53 signaling pathway (hsa04115) (Figure 2B).

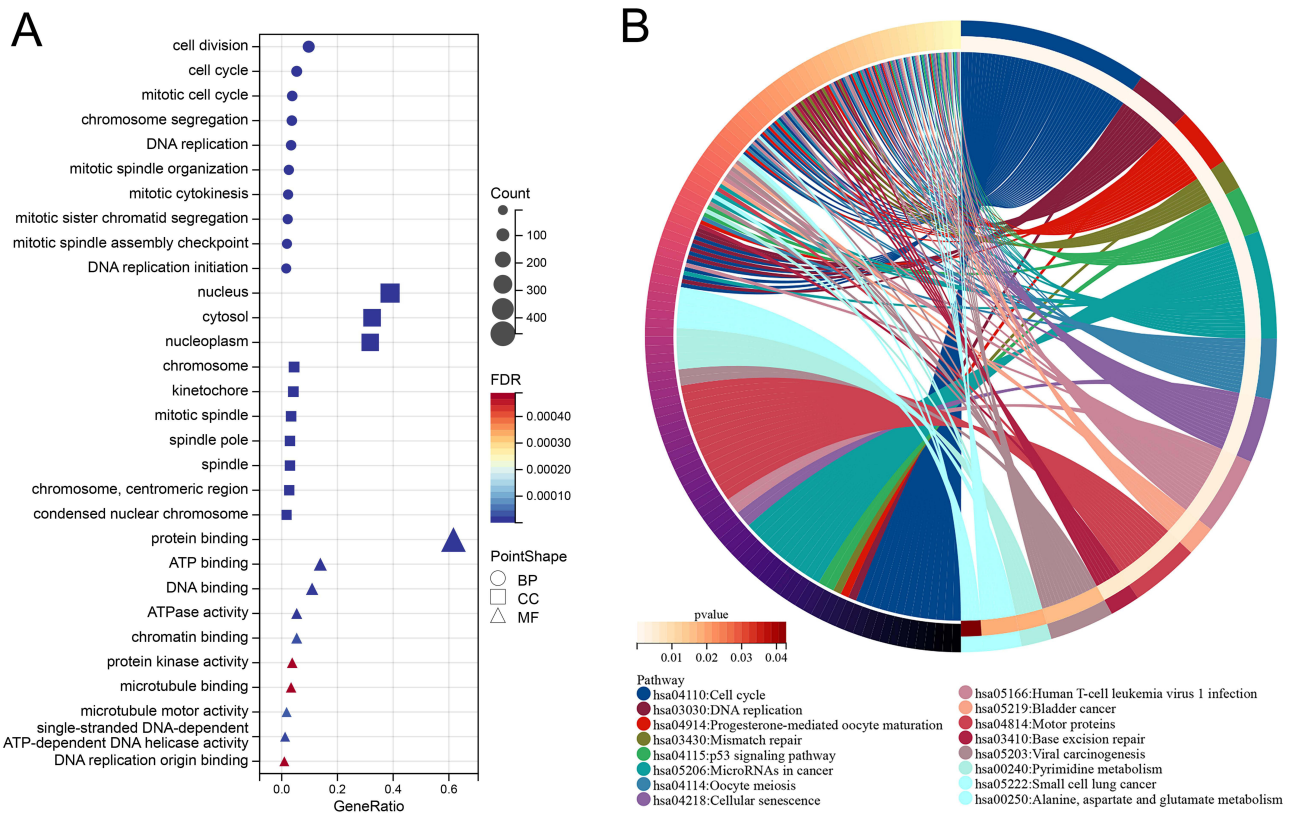

Figure 2 GO and KEGG analyses of TNM stage-related genes in GC. (**A**) Bubble diagram shows the the results of GO analysis. The circle represents BP, the square represents CC, and the triangle represents MF. The larger the node size, the more genes. The darker the blue, the lower the FDR value, and vice versa for red. (**B**) String diagram shows results of KEGG analysis. Different colored lines indicate different items.

Abbreviations: GO, gene ontology; BP, biological process; CC, cellular components; MF, molecular function; FDR, false discovery rate; KEGG, Kyoto Encyclopedia of Genes and Genomes.

Screening of Key Targets Related to GC Progression

Subsequently, univariate Cox regression analysis was performed on 898 genes obtained from the blue and black modules, and 68 genes were found to be significantly associated with survival (Figure 3A). Further, after the analyses of XGBoost (Figure 3B), RF (Figure 3C), and LASSO (Figure 3D), 20, 65 and 25 genes were obtained respectively, and finally 14 targets in the intersection were obtained (Figure 3E), including psoriasis susceptibility 1 candidate 3 (PSORS1C3), AC215219.2, glycerophosphocholine phosphodiesterase 1 (GPCPD1), FYVE, RhoGEF and PH domain containing 6 (FGD6), thiol methyltransferase 1A (TMT1A, also known as METTL7A), SRY-box transcription factor 4(SOX4), FAT1, natural killer cell cytotoxicity receptor 3 ligand 1 (NCR3LG1), NR3C2, SLC1A5, Rho guanine nucleotide exchange factor 37 (ARHGEF37), growth factor receptor bound protein 14 (GRB14), adhesion G protein-coupled receptor L1 (ADGRL1, also known as LPHN1), chromosome 1 open reading frame 226 (C1orf226). Among them, PSORS1C3 and AC215219.2 could not encode proteins. The other 12 candidates were considered to be crucial targets associated with GC progression. Through the GeneMANIA database, we obtained 20 genes co-expressed with the 12 genes mentioned above (Figure 4A). The network relationships among them were analyzed using cytoscope software (Figure 4B). Then cytohubba plug-in was used to calculate the BC, DC, CC, and MCC of these genes, and finally three hub genes were obtained, including NR3C2, FAT1 and SLC1A5 (Figure 4C-D).

The Results of Molecular Docking

Through HERB database, 376 natural components targeting NR3C2, FAT1 and SLC1A5 were found, among which 14 were for SLC1A5, 1 was for FAT1 and 366 were for NR3C2 (Supplementary Table 1). There were 667 components associated with GC (Supplementary Table 2). 23 components were in the intersection. After screening based on the criteria described in the Methods

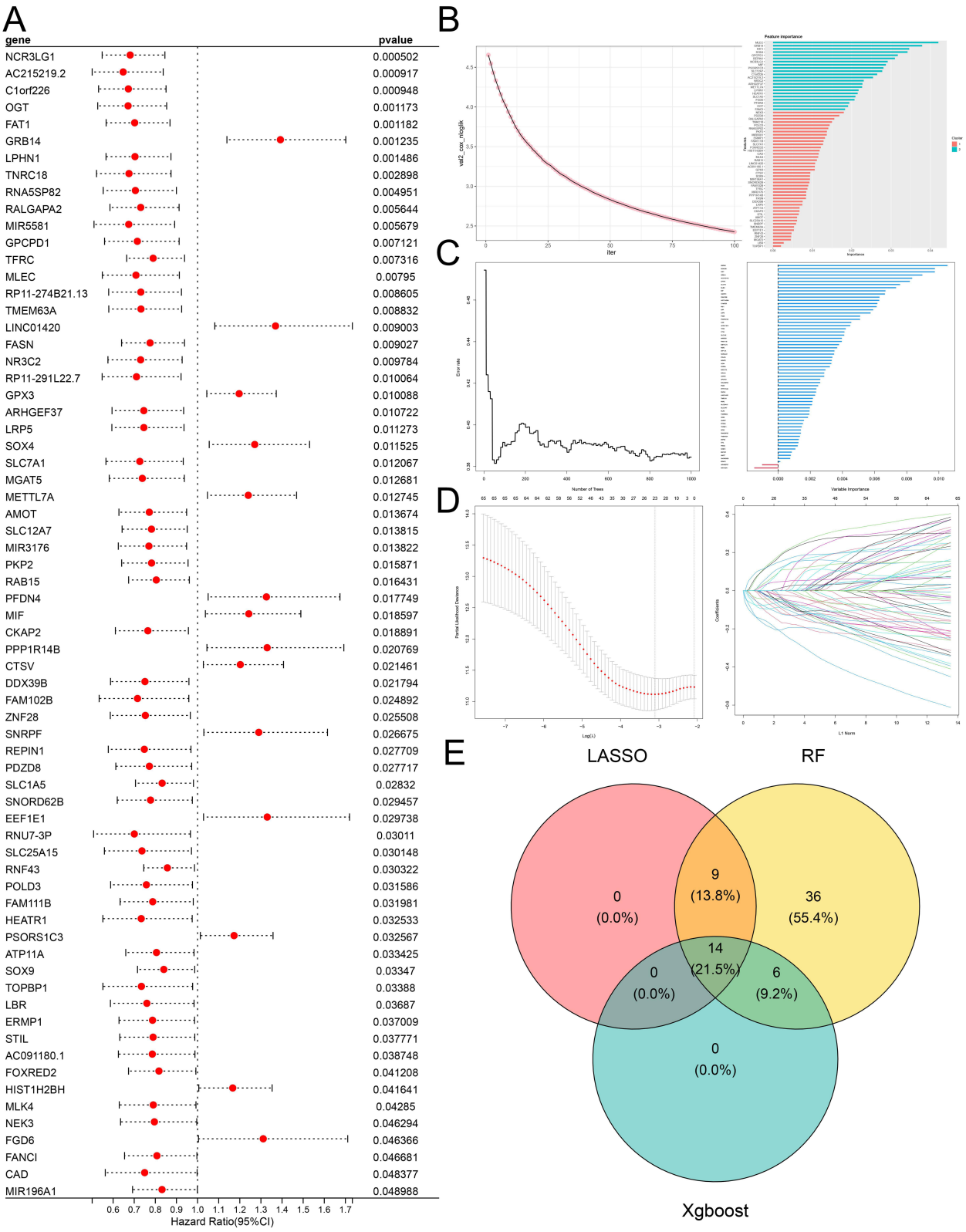

Figure 3 Screening of key genes related to GC progression. (A) Univariate Cox regression of genes in blue and black modules of WGCNA.(B) Feature importance derived from the XGBoost model. (**C**) Random number and variable importance of random forest. (**D**) Optimal parameter (lambda) selection and coefficient distribution for LASSO models of 68 prognostic related genes. (**E**) Venn diagram showing crossover genes after the analyses of XGBoost, RF and LASSO.
Abbreviations: LASSO, least absolute shrinkage and selection operator; RF, random forest.

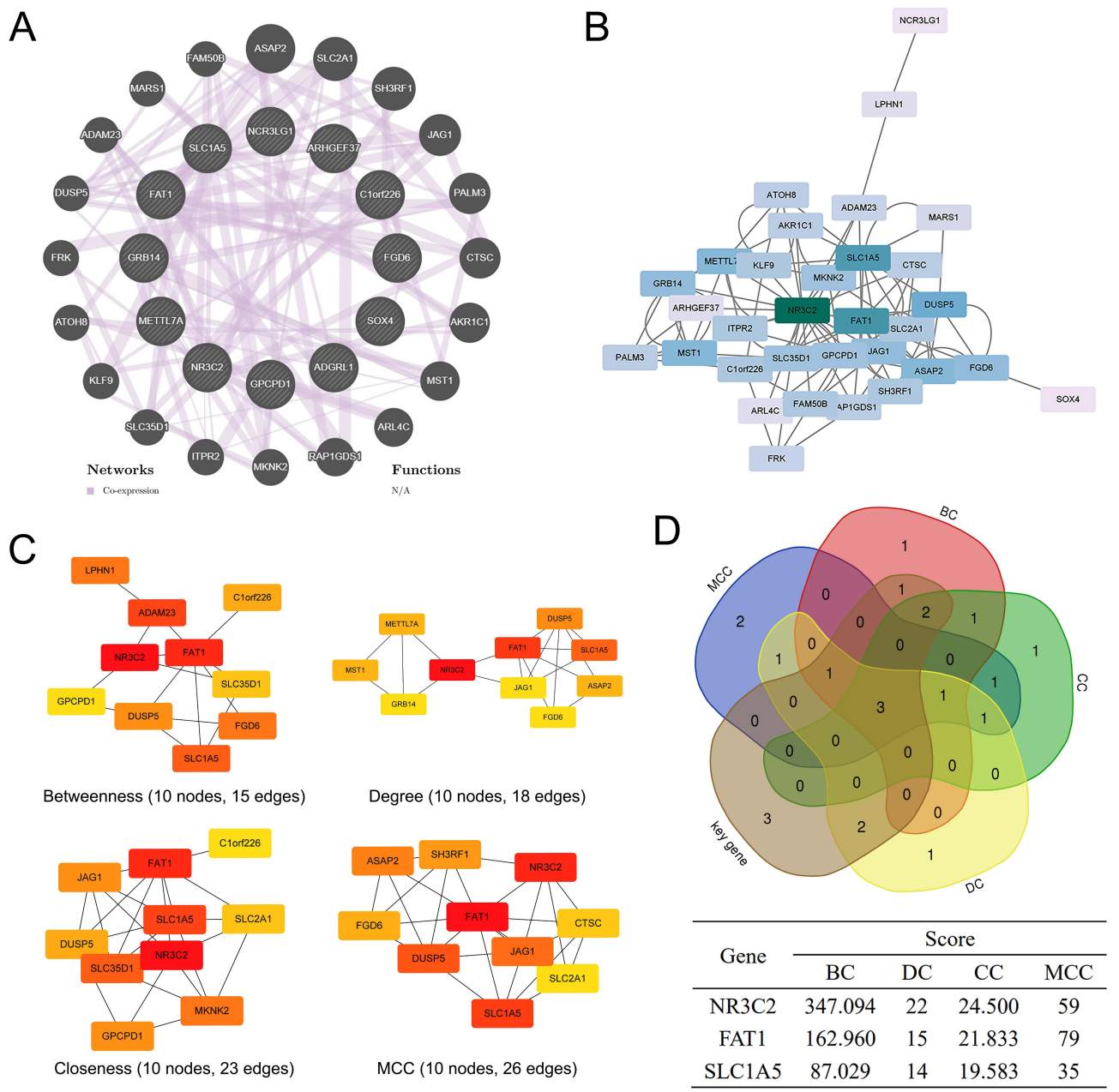

Gene	Score			
	BC	DC	CC	MCC
NR3C2	347.094	22	24.500	59
FAT1	162.960	15	21.833	79
SLC1A5	87.029	14	19.583	35

Figure 4 Further screening of hub genes. (**A**) The co-expressed genes of 12 protein-coding genes were obtained from GeneMANIA database. (**B**)The interaction network between the 12 key genes and their co-expressed genes was demonstrated using cytoscope software. The heavier the node color, the greater the degree value. (**C**) The cytohubba plug-in of cytoscope software was used to calculate BC, DC, CC, and MCC, and the top 10 genes were obtained. (**D**) Venn diagram identified NR3C2, FAT1 and SLC1A5 as the hub genes.

Abbreviations: BC, betweenness; DC, degree; CC, closeness; MCC, Maximal Clique Centrality.

and Materials section, two bioactive components were obtained, deoxycholic acid and diosgenin, which could probably target NR3C2 and SLC1A5 (Table 1; Figure 5A and B). Then molecular docking of deoxycholic acid and diosgenin with hub genes was performed. The results showed that diosgenin interacted with GLU847 residue of NR3C2 to form hydrogen bond (1.9 Å) (Figure 6A). Deoxycholic acid interacted with NR3C2 via HIS841 residues (2.1 Å) and TYR849 residues (2.0 Å) with hydrogen bonding (Figure 6B). Diosgenin interacted with ILE223 residues of SLC1A5 (2.7 Å) and the LEU224 residues (2.0 Å) by forming hydrogen bonds (Figure 6C). Deoxycholic acid interacted with residues of ALA421 (2.3 Å), LEU224 (2.0 Å) and ILE223 (2.3 Å) of SLC1A5 via hydrogen bonding (Figure 6D). Without exception, the binding energy between them was less

Table 1 Pharmacological and Molecular Properties Data of Deoxycholic Acid and Diosgenin in TCMSP Databases

Molecule ID	Molecule name	MW	AlogP	Hdon	Hacc	OB (%)	Caco-2	BBB	DL	FASA-	TPSA	RBN	HL
MOL008845	Deoxycholic acid	392.64	4.06	3	4	40.72	−0.28	−0.88	0.68	0.28	77.76	4	7.01
MOL000546	Diosgenin	414.69	4.63	1	3	80.88	0.82	0.27	0.81	0.19	38.69	0	4.14

Note: MW: molecular weight; AlogP: octanol/water partition coefficient; Hdon: H-bond donor number; Hacc: H-bond acceptor number; OB: oral bioavailability; Caco-2: Caco-2 permeability; BBB: blood-brain barrier; DL: drug-likeness; FASA-: fractional negative accessible surface area; TPSA: topological polar surface area; RBN: rotatable bond numbers; HL: half-life.

than −5 kcal·mol-1, indicating that they have good docking activity. These data suggested that deoxycholic acid and diosgenin were promising drugs to block GC progression via repressing the activity of NR3C2 and SLC1A5.

Expression Characteristics and Prognosis-Prediction Value of SLC1A5 in GC

Through UALCAN database (https://ualcan.path.uab.edu/index.html) and GEPIA database (http://gepia.cancer-pku.cn/), it was revealed that SLC1A5 expression was highly expressed in GC, tissues, compared with that in non-cancer tissues (Figure 7A-B). Additionally, pan-cancer analysis suggested that SLC1A5 was frequently dysregulated in multiple human malignancies (Figure 7C). Consistently, in all of the 10 pairs of GC tissues/adjacent tissues, immunohistochemical analysis showed that the expression of SLC1A5 in tumor tissue (high/low=8/2) was higher than that in non-cancerous tissues (high/low=1/9) (P=0.005, Fisher's exact test) (Figure 7D). In TCGA-STAD dataset, the patients with high SLC1A5 expression had shorter overall survival (Figure 7E). Moreover, SLC1A5 expression had good diagnostic value for 1-year overall survival (AUC=0.63) (Figure 7F). In addition, SLC1A5 expression level was significantly negatively correlated with StromalScore, ImmuneScore, and ESTIMATEScore, indicating that SLC1A5 expression was correlated with immune infiltration (Figure 7G). The results of GSEA showed that abnormal SLC1A5 expression could probably be associated with MYC targets v2 (NES = 2.217, FDR = 0.002), E2F targets (NES = 2.066, FDR = 0.002), MTORC1 signaling (NES = 2.073, FDR = 0.002), unfolded protein response (NES = 2.171, FDR = 0.002), G2M checkpoint (NES =2.045, FDR = 0.003), and DNA repair (NES = 2.116, FDR = 0.003) (Figure 7H). These data suggested that SLC1A5 was a potential oncoprotein in GC, and it could probably function via multiple downstream pathways including mTORC1 signaling.

Diosgenin Regulates Proliferation, Apoptosis and G0/G1 Phase Arrest of GC Cells Through the mTORC1 Signaling

To further verify the effect of diosgenin on the behaviors of GC cells, cell viability, apoptosis, and cell cycle distribution were evaluated. AGS and SNU-16 cells were treated with different concentrations of diosgenin (0, 1, 3, 5, 10, 25, 50 μM)

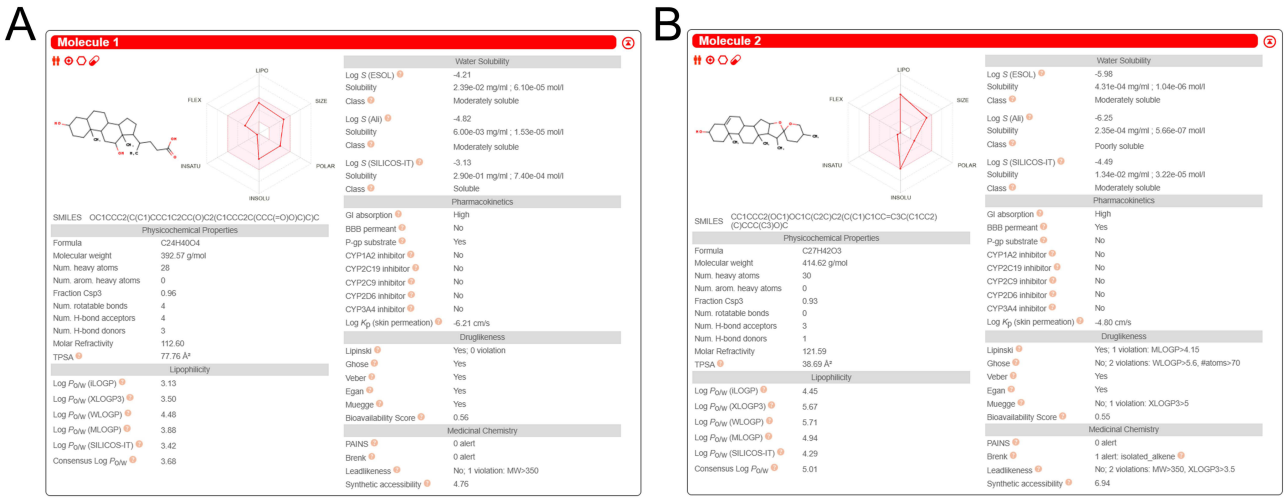

Figure 5 Pharmacological and molecular characteristics of deoxycholic acid (**A**) and diosgenin (**B**) in SwissADME databases.

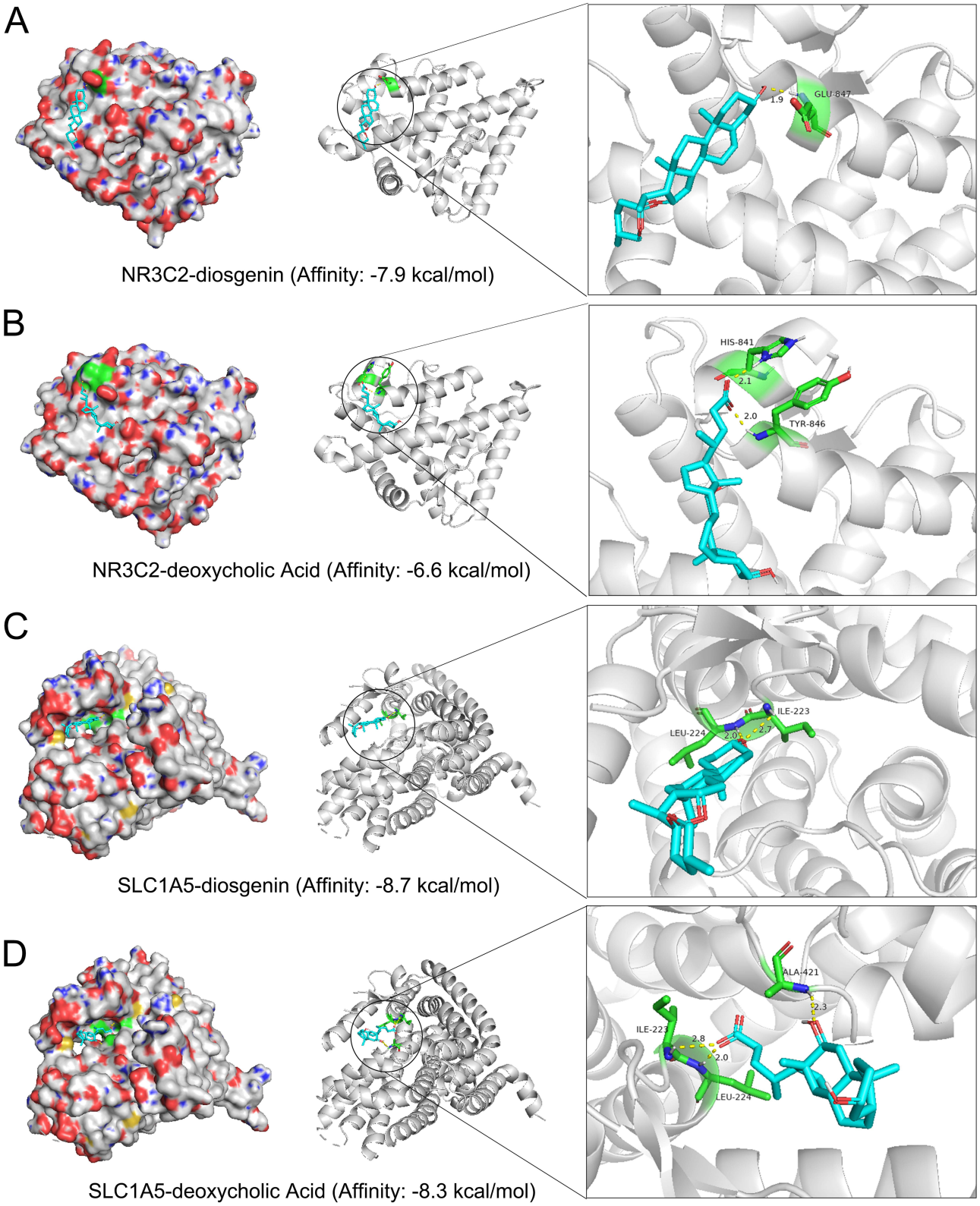

Figure 6 Molecular docking results. (**A**) The binding relationship between NR3C2 and diosgenin. (**B**) The binding relationship between of NR3C2 and deoxycholic acid. (**C**) The binding relationship between of SLC1A5 and diosgenin. (**D**) The binding relationship between SLC1A5 and deoxycholic acid.
Abbreviations: NR3C2, nuclear receptor subfamily 3 group C member 2; SLC1A5, solute carrier family 1 member 5.

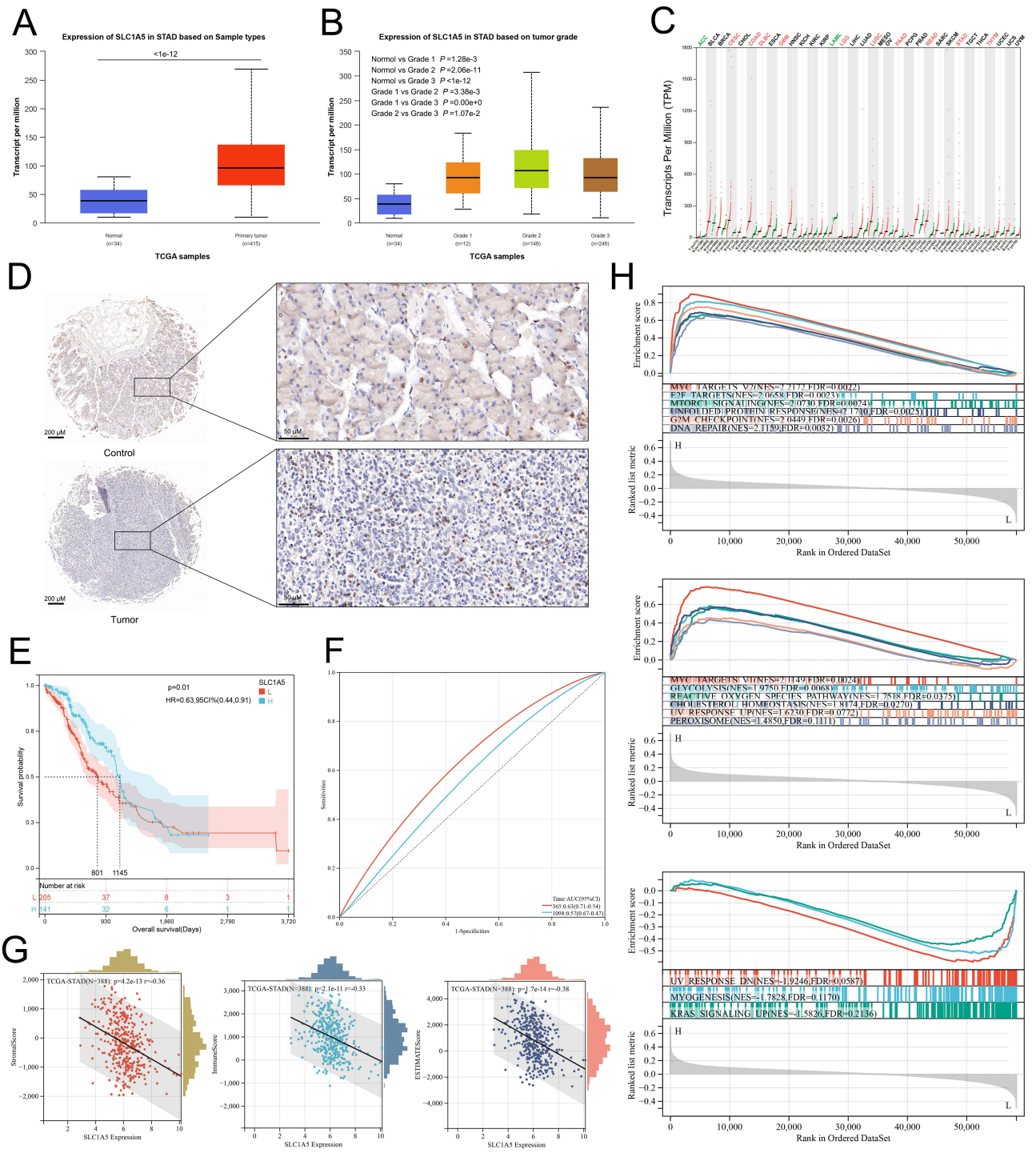

Figure 7 Expression characteristics and clinical significance of SLC1A5. (**A** and **B**). UALCAN database was used to analyze the expression of SLC1A5 in GC tissues. (**C**) The expression of SLC1A5 in pan-cancer was analyzed by GEPIA database.(**D**). The expression of SLC1A5 in 10 pairs of GC tissues and non-cancerous tissues was analyzed by immunohistochemistry, and representative images are provided. (n=10) Bar = 200 μM (left) and 50 μM (right).(**E**). Kaplan–Meier survival analysis for SLC1A5 in the TCGA-STAD dataset. (**F**). ROC analysis for overall survival prediction including 1 and 3 years of GC patients in the TCGA-STAD.(**G**). Correlation analysis between SLC1A5 expression and StromalScore, ImmuneScore, and ESTIMATEScore in TCGA-STAD.(**H**). GSEA of the 15 enriched pathways in GC samples with abnormal SLC1A5 expression.
Abbreviations: ROC, Receiver Operating Characteristic; STAD, Stomach adenocarcinoma; GSEA, Gene set enrichment analyses.

for 48h. The results showed that the viability of AGS and SNU-16 cells gradually decreased with the increase of diosgenin concentration (Figure 8A). The 50% growth inhibition concentration (IC_{50}) of AGS and SNU-16 was 25.46 μM and 19.26 μM, respectively (Figure 8A). Subsequently, AGS and SNU-16 cells were treated with 10 μM diosgenin,

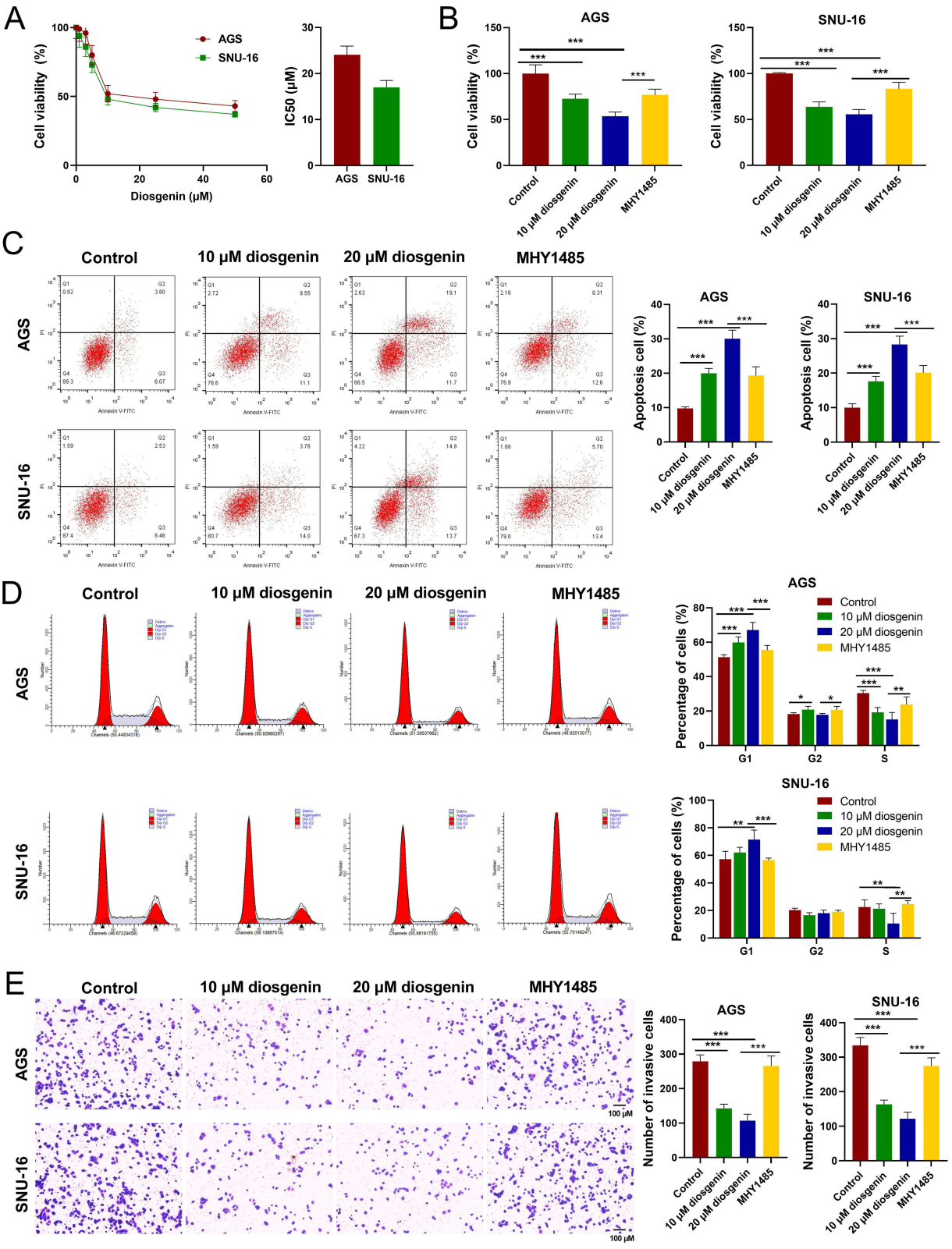

Figure 8 Diosgenin regulates the viability, apoptosis and cycle of GC cells. (**A** and **B**). The viability of AGS and SNU-16 cells was detected by CCK-8 assay (**A**), and the IC_{50} value was calculated (**B** and **C**). Flow cytometry was used to detect the apoptosis of AGS and SNU-16 cells.(**D**). Cell cycle distribution of AGS and SNU-16 was detected by flow cytometry. (**E**) Transwell assay was used to detect the invasive ability of AGS and SNU-16 cells. Bar=100 μM.
Notes: **P*<0.05, ***P*<0.01 and ****P*<0.001.

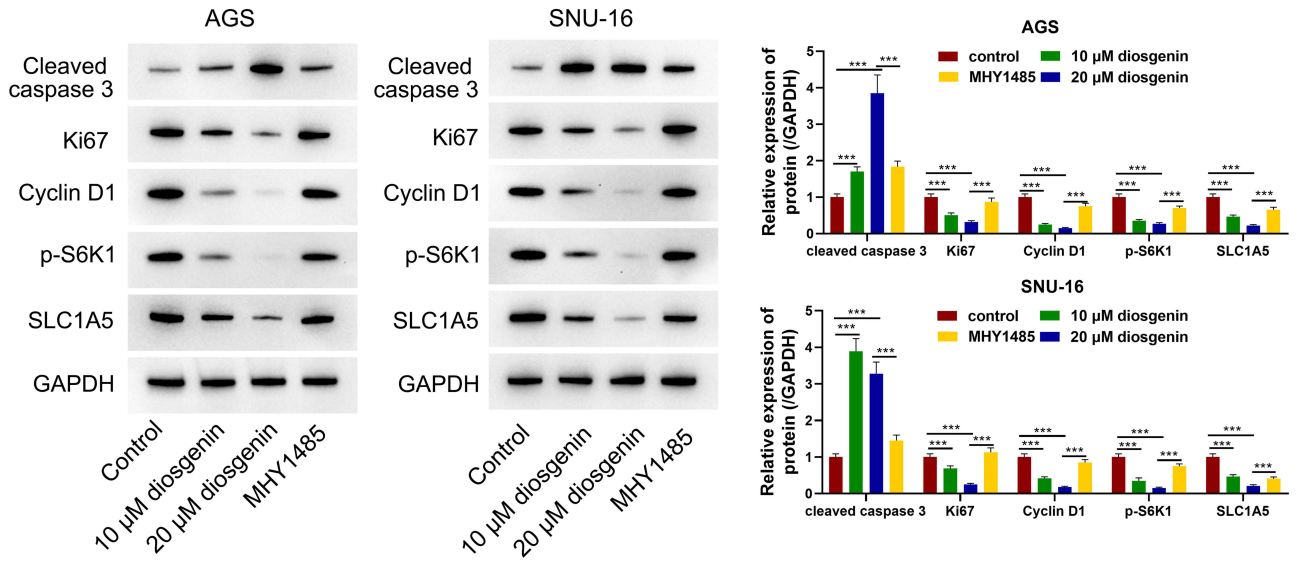

Figure 9 Western blot was used to detect the protein expression levels of cleaved caspase 3, Ki67, cyclin D1, p-S6K1, and SLC1A5 in GC cells.SLC1A5: solute carrier family 1 member 5; GAPDH: glyceraldehyde 3-phosphate dehydrogenase.
Note: ***$P<0.001$.

and 20 μM diosgenin, and 20 μM diosgenin and mTORC1 signaling activator (MHY1485) for 48h, respectively. As shown, diosgenin significantly inhibited the viability of AGS and SNU-16 cells, while MHY1485 treatment significantly reversed this phenomenon, increasing the viability of AGS and SNU-16 cells (Figure 8B). The results of apoptosis and cell cycle experiments showed that diosgenin significantly promoted apoptosis, causing an increase in G1 phase cells and a decrease in S phase cells, while MHY1485 treatment reversed this phenomenon (Figure 8C-D). The results of Transwell assay showed that diosgenin treatment group significantly reduced the invasion of GC cells, and the MHY1485 co-treatment partially reversed this phenomenon (Figure 8E). Western blot showed that diosgenin promoted cleaved caspase 3 expression and inhibited the expression levels of Ki67, cyclin D1, p-S6K1 and SLC1A5, and the phenomena were reversed after MHY1485 treatment (Figure 9).

Discussion

Although treatment methods such as surgery, chemotherapy, radiotherapy and immunotherapy have improved the prognosis of GC patients, the clinical outcome of most GC patients is still poor due to the difficulty of early diagnosis, the unsatisfactory therapeutic effect, and the ease of distant metastasis and recurrence.[33] It is important to clarify the molecular mechanism of GC progression to develop new treatment strategies. In this study, with WGCNA, a total of 898 genes were revealed to be significantly correlated with TNM staging of GC patients. Next, three GC prognostic genes, namely NR3C2, FAT1 and SLC1A5, were obtained by three machine learning algorithms. NR3C2 is a nuclear transcription factor that encodes the MR protein (also known as mineralocorticoid receptor).[34] A number of studies have indicated that NR3C2 is down-regulated in cancer and has a cancer-inhibiting effect.[35,36] NR3C2 can inhibit the proliferation and epithelial-mesenchymal transition (EMT) of pancreatic cancer cells and increase their sensitivity to certain chemotherapy agents.[37] EMT plays a critical role in cancer metastasis.[38] In hepatocellular carcinoma, NR3C2 regulates β-catenin signal transduction pathways.[39] NR3C2 inhibits the proliferation of colorectal cancer by regulating glucose metabolism and phosphorylating AMPK.[36] FAT1 encodes proto-cadherin and is one of the commonly mutated genes in human cancer.[40] FAT1 deletion promotes malignant progression by controlling cell polarity and adhesion between tumor cells and between tumor cells and extracellular matrix.[41] In addition, FAT1 is involved in regulating the activation of EGFR-RAS-RAF-MEK-MAPK, EGFR-PI3K-AKT-MTOR and Hippo signaling pathways.[41,42] Considering NR3C2 and FAT1 are commonly regarded as tumor suppressors in cancer biology, in the present work, SLC1A5 was selected as the research emphasis as a drug target.

SLC1A5 is a solute transporter on the cell surface that mediates the uptake of neutral amino acids, including glutamine.[43] In cancer cells, the demand for glutamine increases dramatically. L-glutamine is the main nitrogen source for the synthesis of amino acids, nucleotides and lipids, as well as the carbon source for the tricarboxylic acid (TCA) cycle and cellular energy required for cancer cell growth.[44] L-glutamine is introduced into cells to provide fuel for energy and anabolic pathways through SLC1A5,[45] and SLC1A5 plays a key role in metabolic reprogramming of cancer cells.[46] Previous studies have confirmed that blocking SLC1A5 to prevent glutamine uptake successfully prevents the proliferation of tumor cells in melanoma,[47] non-small cell lung cancer,[48,49] breast cancer,[50] and acute myeloid leukemia.[51] In the present work, it was found that SLC1A5 was highly expressed in GC, which was closely related with tumor grade and immune cell infiltration. In addition, patients with higher SLC1A5 expression had shorter survival. Bioinformatics analysis showed that SLC1A5 expression was closely related to MYC targets v2, E2F targets, MTORC1 signaling, G2M checkpoint, etc. These data suggested that SLC1A5 was a promising drug target for GC, which may have similar oncogenic properties with its role in other cancers.[47–51]

In this work, two potential natural bioactive compounds for GC treatment (deoxycholic acid and diosgenin) were obtained. Deoxycholic acid is an active ingredient in indigoplant leaf, cow-bezoar, fortune plumyew and bear gall.[52,53] It can induce metaplasia of gastric epithelium by activating STAT3 signal transduction and disrupting gastric bile acid metabolism and microbiota, which affects the occurrence of GC.[54] Diosgenin, a natural steroid saponin, is an important precursor of steroid hormones and has high medicinal value.[10] The invasion process is one of the key drivers of cancer metastasis.[55,56] In this study, it was observed that diosgenin significantly inhibited the viability and invasion ability of GC cells. Diosgenin can induce apoptosis, DNA damage, and modulate mitochondrial signaling pathways.[57] In GC, previous studies have confirmed that diosgenin can induce G0/G1 cell cycle arrest and apoptosis of cancer cells.[17] Consistently, we observed that diosgenin blocked cell cycle progression and induced apoptosis of GC cells.

In this study, we confirmed that diosgenin has good binding activity with SLC1A5. In vitro experiments confirmed that diosgenin promoted cleaved caspase-3 expression and inhibited the expression levels of Ki67, cyclin D1, p-S6K1 and SLC1A5. Cyclin D1 is an important regulator of the cell cycle, and an allosteric regulator of cyclin dependent kinase 4 (CDK) and CDK6, promoting cell transition from G1 phase to S phase.[58,59] mTOR enhances protein synthesis by forming two different kinase complexes, mTORC1 and mTORC2, respectively, and S6K1 is the substrate downstream of mTORC1, which can bind mRNA with EIF-4E-binding protein 1 (4E-BP1) and regulate the initiation and progression of mRNA translation, thus enhancing protein synthesis and promoting cell proliferation.[60] Some previous studies have validated that SLC1A5 is required for the activation of mTOR signaling.[61,62] Our data showed that diosgenin suppressed the malignant biological behaviors of GC cells via modulating SLC1A5/mTORC1 axis, implying diosgenin is a promising drug to block metabolic reprogramming of cancer cells, and inhibit GC progression.

Conclusion

SLC1A5 contributes to GC progression, and diosgenin may target it to repress the malignant phenotype of GC cells. In the following work, the biological functions of SLC1A5 and diosgenin in regulating GC cells' phenotypes should be further validated by in vivo models.

Data Sharing Statement

The data used to support the findings of this study are available from the corresponding author upon request.

Ethics Statement

All study protocol was approved by the Clinical Research Ethics Committee of Wuhan University People's Hospital. All experiments were performed in compliance with the Declaration of Helsinki, and all patients provided written informed consent.

Funding

This study was supported by Hubei Provincial Natural Science Foundation (No.2021CFB087 and No.2023AFB690).

Disclosure

The authors declare that they have no competing interests.

References

1. Siegel RL, Miller KD, Wagle NS, Jemal A. Cancer statistics, 2023. *Ca a Cancer J Clinicians*. 2023;73(1):17–48. doi:10.3322/caac.21763
2. Gao JP, Xu W, Liu WT, Yan M, Zhu Z-G. Tumor heterogeneity of gastric cancer: from the perspective of tumor-initiating cell. *World J Gastroenterol*. 2018;24(24):2567–2581. doi:10.3748/wjg.v24.i24.2567
3. Sung H, Ferlay J, Siegel RL, et al. Global Cancer Statistics 2020: GLOBOCAN Estimates of Incidence and Mortality Worldwide for 36 Cancers in 185 Countries. *Ca a Cancer J Clinicians*. 2021;71(3):209–249. doi:10.3322/caac.21660
4. Machlowska J, Baj J, Sitarz M, Maciejewski R, Sitarz R. Gastric cancer: epidemiology, risk factors, classification, genomic characteristics and treatment strategies. *Int J Mol Sci*. 2020;21(11):4012. doi:10.3390/ijms21114012
5. Japanese Gastric Cancer Association. Japanese gastric cancer treatment guidelines 2018. *Gastric Cancer*. 2021;24(1):1–21. doi:10.1007/s10120-020-01042-y
6. Chen D, Chen H, Chi L, et al. Association of tumor-associated collagen signature with prognosis and adjuvant chemotherapy benefits in patients with gastric cancer. *JAMA network open*. 2021;4(11):e2136388. doi:10.1001/jamanetworkopen.2021.36388
7. Jiang Y, Li T, Liang X, et al. Association of adjuvant chemotherapy with survival in patients with stage II or III gastric cancer. *JAMA Surgery*. 2017;152(7):e171087. doi:10.1001/jamasurg.2017.1087
8. Chen Y, Tang YM, Yu SL, et al. Advances in the pharmacological activities and mechanisms of diosgenin. *Chinese J Nat Med*. 2015;13(8):578–587. doi:10.1016/S1875-5364(15)30053-4
9. Selim S, Al Jaouni S. Anticancer and apoptotic effects on cell proliferation of diosgenin isolated from costus speciosus (Koen.) Sm. *BMC Complement Altern Med*. 2015;15:301. doi:10.1186/s12906-015-0836-8
10. Sautour M, Mitaine-Offer AC, Miyamoto T, Dongmo A, Lacaille-Dubois MA. A new steroidal saponin from Dioscorea cayenensis. *Chem. Pharm. Bull.* 2004;52(11):1353–1355. doi:10.1248/cpb.52.1353
11. Arya P, Kumar P. Diosgenin: an ingress towards solving puzzle for diabetes treatment. *J Food Biochem*. 2022;46(12):e14390. doi:10.1111/jfbc.14390
12. Li X, Liu S, Qu L, et al. Dioscin and diosgenin: insights into their potential protective effects in cardiac diseases. *J Ethnopharmacol*. 2021;274:114018. doi:10.1016/j.jep.2021.114018
13. Parama D, Boruah M, Yachna K, et al. Diosgenin, a steroidal saponin, and its analogs: effective therapies against different chronic diseases. *Life Sci*. 2020;260:118182. doi:10.1016/j.lfs.2020.118182
14. Raju J, Bird RP. Diosgenin, a naturally occurring steroid [corrected] saponin suppresses 3-hydroxy-3-methylglutaryl CoA reductase expression and induces apoptosis in HCT-116 human colon carcinoma cells. *Cancer Lett*. 2007;255(2):194–204. doi:10.1016/j.canlet.2007.04.011
15. Ren QL, Wang Q, Zhang XQ, et al. Anticancer activity of diosgenin and its molecular mechanism. *Chin J Integr Med*. 2023;29(8):738–749. doi:10.1007/s11655-023-3693-1
16. Sethi G, Shanmugam MK, Warrier S, et al. Pro-apoptotic and anti-cancer properties of diosgenin: a comprehensive and critical review. *Nutrients*. 2018;10(5):645. doi:10.3390/nu10050645
17. Liu S, Rong G, Li X, et al. Diosgenin and GSK126 produce synergistic effects on epithelial-mesenchymal transition in gastric cancer cells by mediating EZH2 via the Rho/ROCK signaling pathway. *Onco Targets Ther*. 2020;13:5057–5067.
18. Hernández-Vázquez JMV, López-Muñoz H, Escobar-Sánchez ML, et al. Apoptotic, necrotic, and antiproliferative activity of diosgenin and diosgenin glycosides on cervical cancer cells. *Eur J Pharmacol*. 2020;871:172942. doi:10.1016/j.ejphar.2020.172942
19. Langfelder P, Horvath S. WGCNA: an R package for weighted correlation network analysis. *BMC Bioinf*. 2008;9:559. doi:10.1186/1471-2105-9-559
20. Chen T, He Q, Xiang Z, Dou R, Xiong B. Identification and validation of key genes of differential correlations in gastric cancer. *Front Cell Develop Biol*. 2021;9:801687. doi:10.3389/fcell.2021.801687
21. Rezaei Z, Ranjbaran J, Safarpour H, et al. Identification of early diagnostic biomarkers via WGCNA in gastric cancer. *Biomed Pharmacother*. 2022;145:112477. doi:10.1016/j.biopha.2021.112477
22. Feng S, Xu Y, Dai Z, et al. Integrative analysis from multicenter studies identifies a WGCNA-derived cancer-associated fibroblast signature for ovarian cancer. *Front Immunol*. 2022;13:951582. doi:10.3389/fimmu.2022.951582
23. Vafaeie F, Nomiri S, Ranjbaran J, Safarpour H. ACAN, MDFI, and CHST1 as candidate genes in gastric cancer: a comprehensive insilco analysis. *Asian Pacific J Cancer Prevent*. 2022;23(2):683–694. doi:10.31557/APJCP.2022.23.2.683
24. Wang T, Dai L, Shen S, et al. Comprehensive molecular analyses of a macrophage-related gene signature with regard to prognosis, immune features, and biomarkers for immunotherapy in hepatocellular carcinoma based on WGCNA and the LASSO Algorithm. *Front Immunol*. 2022;13:843408. doi:10.3389/fimmu.2022.843408
25. Zheng H, Liu H, Li H, et al. Characterization of stem cell landscape and identification of stemness-relevant prognostic gene signature to aid immunotherapy in colorectal cancer. *Stem Cell Res Ther*. 2022;13(1):244. doi:10.1186/s13287-022-02913-0
26. G D, Sherman BT, Hosack DA, et al. DAVID: database for annotation, visualization, and integrated discovery. *Genome Biol*. 2003;4(5):3. doi:10.1186/gb-2003-4-5-p3
27. Shen W, Song Z, Zhong X, et al. Sangerbox: a comprehensive, interaction-friendly clinical bioinformatics analysis platform. *Imeta*. 2022;1(3):e36. doi:10.1002/imt2.36
28. Ishwaran H, Lauer MS, Blackstone EH, Lu M, Kogalur UB. Randomforestsrc: random survival forests vignette. *Random Forest SRC*. 2022;15:1
29. Friedman J, Hastie T, Tibshirani R. Regularization paths for generalized linear models via coordinate descent. *Journal of Statistical Software*. 2010;33(1):1–22. doi:10.18637/jss.v033.i01
30. Chen T, Guestrin C. Xgboost: a scalable tree boosting system, Proceedings of the 22nd acm sigkdd international conference on knowledge discovery and data mining. 2016;1:785–794.
31. Franz M, Rodriguez H, Lopes C, et al. GeneMANIA update 2018. *Nucleic Acids Res*. 2018;46(W1):W60–w64. doi:10.1093/nar/gky311

32. Chin C-H, Chen S-H, Wu -H-H, et al. cytoHubba: identifying hub objects and sub-networks from complex interactome. *BMC Syst. Biol.* 2014;8 (4):1–7. doi:10.1186/1752-0509-8-S4-S11
33. Thrift AP, El-Serag HB. Burden of gastric cancer, Clinical gastroenterology and hepatology: the official clinical practice. *J Am Gastroenterol Assoc*. 2020;18(3):534–542.
34. Li J, Xu Z. NR3C2 suppresses the proliferation, migration, invasion and angiogenesis of colon cancer cells by inhibiting the AKT/ERK signaling pathway. *Mol Med Rep*. 2022;25(4):133. doi:10.3892/mmr.2022.12649
35. Fan Y, Li Y, Zhu Y, et al. miR-301b-3p regulates breast cancer cell proliferation, migration, and invasion by targeting NR3C2. *J Oncol*. 2021;2021:8810517. doi:10.1155/2021/8810517
36. Liu H, Lei W, Li Z, Wang X, Zhou L. NR3C2 inhibits the proliferation of colorectal cancer via regulating glucose metabolism and phosphorylating AMPK. *J Cell & Mol Med*. 2023;27(8):1069–1082. doi:10.1111/jcmm.17706
37. Yang S, He P, Wang J, et al. A novel MIF signaling pathway drives the malignant character of pancreatic cancer by targeting NR3C2. *Cancer Res*. 2016;76(13):3838–3850. doi:10.1158/0008-5472.CAN-15-2841
38. Li D, Xia L, Huang P, et al. Heterogeneity and plasticity of epithelial-mesenchymal transition (EMT) in cancer metastasis: focusing on partial EMT and regulatory mechanisms. *Cell Proliferation*. 2023;56(6):e13423. doi:10.1111/cpr.13423
39. Yang C, Ma X, Guan G, et al. MicroRNA-766 promotes cancer progression by targeting NR3C2 in hepatocellular carcinoma. *FASEB J*. 2019;33 (1):1456–1467. doi:10.1096/fj.201801151R
40. ICGC/TCGA Pan-Cancer Analysis of Whole Genomes Consortium. Pan-cancer analysis of whole genomes. *Nature*. 2020;578(7793):82–93. doi:10.1038/s41586-020-1969-6
41. Pastushenko I, Mauri F, Song Y, et al. Fat1 deletion promotes hybrid EMT state, tumour stemness and metastasis. *Nature*. 2021;589(7842):448–455. doi:10.1038/s41586-020-03046-1
42. Lu Y, Wang Z, Zhou L, et al. FAT1 and PTPN14 regulate the malignant progression and chemotherapy resistance of esophageal cancer through the hippo signaling pathway. *Analy Cell Pathol*. 2021;2021:9290372.
43. Kanai Y, Hediger MA. The glutamate/neutral amino acid transporter family SLC1: molecular, physiological and pharmacological aspects. *Pflugers Archiv*. 2004;447(5):469–479. doi:10.1007/s00424-003-1146-4
44. DeBerardinis RJ, Lum JJ, Hatzivassiliou G, Thompson CB. The biology of cancer: metabolic reprogramming fuels cell growth and proliferation. *Cell Metab*. 2008;7(1):11–20. doi:10.1016/j.cmet.2007.10.002
45. Luo M, Wu L, Zhang K, et al. miR-137 regulates ferroptosis by targeting glutamine transporter SLC1A5 in melanoma. *Cell Death Differ*. 2018;25 (8):1457–1472. doi:10.1038/s41418-017-0053-8
46. Yoo HC, Park SJ, Nam M, et al. A Variant of SLC1A5 is a mitochondrial glutamine transporter for metabolic reprogramming in cancer cells. *Cell Metab*. 2020;31(2):267–283.e12. doi:10.1016/j.cmet.2019.11.020
47. Wang Q, Beaumont KA, Otte NJ, et al. Targeting glutamine transport to suppress melanoma cell growth. *Int J Cancer*. 2014;135(5):1060–1071. doi:10.1002/ijc.28749
48. Zhang Y, Dong P, Liu N, et al. TRIM6 reduces ferroptosis and chemosensitivity by targeting SLC1A5 in lung cancer. *Oxid Med Cell Longev*. 2023;2023:9808100.
49. Hassanein M, Hoeksema MD, Shiota M, et al. SLC1A5 mediates glutamine transport required for lung cancer cell growth and survival. *Clin Cancer Res*. 2013;19(3):560–570. doi:10.1158/1078-0432.CCR-12-2334
50. van Geldermalsen M, Wang Q, Nagarajah R, et al. ASCT2/SLC1A5 controls glutamine uptake and tumour growth in triple-negative basal-like breast cancer. *Oncogene*. 2016;35(24):3201–3208. doi:10.1038/onc.2015.381
51. Weng H, Huang F, Yu Z, et al. The m(6)A reader IGF2BP2 regulates glutamine metabolism and represents a therapeutic target in acute myeloid leukemia. *Cancer Cell*. 2022;40(12):1566–1582.e10. doi:10.1016/j.ccell.2022.10.004
52. Qiao X, Ye M, Pan DL, et al. Differentiation of various traditional Chinese medicines derived from animal bile and gallstone: simultaneous determination of bile acids by liquid chromatography coupled with triple quadrupole mass spectrometry. *J Chromatogr A*. 2011;1218(1):107–117. doi:10.1016/j.chroma.2010.10.116
53. Chen D, Lin S, Xu W, et al. Qualitative and quantitative analysis of the major constituents in shexiang tongxin dropping pill by HPLC-Q-TOF-MS /MS and UPLC-QqQ-MS/MS. *Molecules*. 2015;20(10):18597–18619. doi:10.3390/molecules201018597
54. Jin D, Huang K, Xu M, et al. Deoxycholic acid induces gastric intestinal metaplasia by activating STAT3 signaling and disturbing gastric bile acids metabolism and microbiota. *Gut Microbes*. 2022;14(1):2120744. doi:10.1080/19490976.2022.2120744
55. Lusby R, Dunne P, Tiwari VK. Tumour invasion and dissemination. *Biochem. Soc. Trans.* 2022;50(3):1245–1257. doi:10.1042/BST20220452
56. Matsuoka T, Yashiro M. Molecular insight into gastric cancer invasion-current status and future directions. *Cancers*. 2023;16(1):54. doi:10.3390/ cancers16010054
57. Lv L, Zheng L, Dong D, et al. Dioscin, a natural steroid saponin, induces apoptosis and DNA damage through reactive oxygen species: a potential new drug for treatment of glioblastoma multiforme. *Food Chem Toxicol*. 2013;592013:657–669.
58. Montalto FI, De Amicis F. Cyclin D1 in cancer: a molecular connection for cell cycle control, adhesion and invasion in tumor and stroma. *Cells*. 2020;9(12):2648. doi:10.3390/cells9122648
59. Li D, Shen L, Zhang X, et al. LncRNA ELF3-AS1 inhibits gastric cancer by forming a negative feedback loop with SNAI2 and regulates ELF3 mRNA stability via interacting with ILF2/ILF3 complex. *J Exp Clin Cancer Res*. 2022;41(1):332. doi:10.1186/s13046-022-02541-9
60. Zoncu R, Efeyan A, Sabatini DM. Sabatini, mTOR: from growth signal integration to cancer, diabetes and ageing, *Nature reviews*. *Mol Cell Biol*. 2011;12(1):21–35. doi:10.1038/nrm3025
61. Zhao X, Petrashen AP, Sanders JA, Peterson AL, Sedivy JM. SLC1A5 glutamine transporter is a target of MYC and mediates reduced mTORC1 signaling and increased fatty acid oxidation in long-lived Myc hypomorphic mice. *Aging Cell*. 2019;18(3):e12947. doi:10.1111/acel.12947
62. Beaumatin F, O'Prey J, Barthet VJA, et al. mTORC1 activation requires DRAM-1 by facilitating lysosomal amino acid efflux. *Mol Cell*. 2019;76 (1):163–176.e8. doi:10.1016/j.molcel.2019.07.021